Environmental Advances 12 (2023) 100381

Contents lists available at ScienceDirect

Environmental Advances

journal homepage: www.sciencedirect.com/journal/environmental-advances

A comprehensive physicochemical characterization of zinc oxide nanoparticles extracted from sunscreens and wastewaters

Anwar Ul Haq Khan [a,b], Yanju Liu [a,b,*], Cheng Fang [a,b], Ravi Naidu [a,b], Ho Kyong Shon [c], Zoe Rogers [d], Rajarathnam Dharmarajan [e]

[a] Global Centre for Environmental Remediation (GCER), College of Engineering Science and Environment, The University of Newcastle, Callaghan, NSW 2308, Australia
[b] crc for Contamination Assessment and Remediation of the Environment (crcCARE), ATC Building, The University of Newcastle, Callaghan, NSW 2308, Australia
[c] School of Civil and Environmental Engineering, University of Technology Sydney (UTS), City Campus, Broadway, NSW 2007, Australia
[d] Hunter Water Corporation, 36 Honeysuckle Drive, Newcastle, NSW 2300, Australia
[e] Australian Centre for Water and Environmental Biotechnology (ACWEB), The University of Queensland, Australia

ARTICLE INFO

Keywords:
Zinc oxide nanoparticles
Sunscreens
Wastewaters
Aging

ABSTRACT

The widespread popularity of sunscreens contributes significantly to the release of zinc oxide (ZnO) nanoparticles into bodies of water, yet there is still lack of sufficient understanding on the realistic behaviour and long-term exposure. In this study, a simple and effective method was used to extract ZnO nanoparticles from ZnO-based sunscreen products (available in Australia) that end up in wastewaters. The extracted ZnO nanoparticles were negative charged at controlled pH 7. Transmission electron microscopy (TEM) analysis revealed an irregular, spherical and rod-shaped nanoparticles extracted from sunscreens and wastewaters with size ≥100 nm. Various nanoparticles containingZnO, iron, silver, and titanium were detected in wastewater samples collected from treatment plants. Other contaminants were also found in the wastewater samples based on TEM elemental analysis. The results documented in this study are useful to understand the presence and characterizations of ZnO nanoparticles in sunscreens and wastewaters. With this knowledge, we can realistically investigate the fate, behaviours and adverse effects of ZnO nanoparticles.

1. Introduction

Ultraviolet absorbance with a high refractive index of metal oxide-based mineral filters such as zinc oxide (ZnO) nanoparticles is usually employed in sunscreen products to protect the human skin from sunburn (Bairi et al., 2017). Commercially available metal oxides such as ZnO-based sunscreens in Australia generally consist of organic and/or inorganic ultraviolet filters that serve to provide sufficient skin protection from skin cancer-causing sunlight (Bairi et al., 2017). ZnO nanoparticles are employed as a colorant and bulking agent. The function of ZnO nanoparticles in sunscreens is to absorb ultraviolet radiation to reduce, eliminate and/or prevent sunburn and premature aging of the skin (Cole et al., 2016; Guedens et al., 2014).

ZnO nanoparticles are widely used in paints, pigments, personal care products such as baby lotions, make-up, bath soaps, nail products, foot powders and other cosmetics including sunscreens (Mohammed et al., 2019). The United States Food and Drug Administration (FDA) recommended that safe cosmetics products containing these white minerals (ZnO nanoparticles) should have concentrations no more than 25% of the total. According to the FDA, the protection against ultraviolet A should be at the minimum one-third of the overall sun protection factor (Smijs and Pavel, 2011).

Traditionally, ZnO nanoparticles such as metal oxide-based filters have been employed in very small amounts (micron to nano units). A study based on the characterizations of metal-based (such as ZnO nanoparticles) filters in commercial sunscreens was conducted by measuring their sizes using techniques such as single particle inductively coupled plasma (sp-ICPMS), transmission electron microscopy (TEM) and X-ray diffraction (XRD) (Lu et al., 2018). The sp-ICPMS proved to be a highly effective and accurate technique for examining the nanoparticles size followed by TEM (Lu et al., 2018). The rising usage of these filters such as ZnO nanoparticles at such nanoscale units poses long-term problems in aquatic systems (Adler and DeLeo, 2020; Bairi et al., 2017; Ramos et al., 2016). Globally, the concentrations of inorganic filters

* Corresponding author at: Global Centre for Environmental Remediation (GCER), College of Engineering Science and Environment, The University of Newcastle, Callaghan, NSW 2308, Australia.
E-mail address: yanju.liu@newcastle.edu.au (Y. Liu).

https://doi.org/10.1016/j.envadv.2023.100381
Received 17 February 2023; Received in revised form 16 May 2023; Accepted 17 May 2023
Available online 19 May 2023

have been detected in marine eco-systems. The concentrations levels vary based on several factors such as area, time, date and number of swimmers (Chatzigianni et al., 2022). The concentrations of thirteen ultraviolet filters were measured in water (surface seawater), sediment, and coral tissue from nineteen locations in Oahu, Hawaii. At the minimum eight ultraviolet filters were detected in seawater, sediment, and coral tissue and overall mass concentrations of all ultraviolet filters were with concentrations < 750 ng/L, < 70 ng/g dry weight, and < 995 ng/g dry weight respectively (Mitchelmore et al., 2019).

Moreover, a percentage of ZnO nanoparticles is expected to be released into bodies of water after passing through wastewater treatment plants (Chauque et al., 2016). For instance, a study based on the simulated wastewater treatment plant described the impacts of ZnO nanoparticles on the wastewater treatment plant associated with the disposal of ZnO nanoparticles. The concentrations of zinc residue in the treated effluent were in the range from 50 to 200 μg/L compared to the zinc in sludge at about 3000 mg/Kg due to their high precipitation levels in the sludge during treatment processes (Chauque et al., 2016).

Due to continuous and rapid increase in the manufacture and application of ZnO nanoparticles, the increase in the environmental concentration of these nanoparticles is inevitably expected. The concentration of these nanoparticles in municipal wastewater is expected to be in the mg/L level in the next few years (Tan et al., 2015). The presence of ZnO nanoparticles in the treatment plants, may obstruct the bacterial activities in the activated sludge and influence the treatment efficiency (Tan et al., 2015). For instance, it is reported that in a sequencing batch reactor the concentration (5 mg/L) of ZnO nanoparticles substantially inhibit the nitrifying activity and result in decrease for the removal of NH_4^+−N in the reactor (Hou et al., 2013). Consequently, these particles are able to accumulate in environmental samples, where toxic effects on some organisms can occur (Attia et al., 2018; Osmond and McCall, 2010; Zheng et al., 2019) and changes the fate and behaviours are possible after interacting with co-existing substances (Khan et al., 2023, 2021).

The presence of ZnO nanoparticles in wastewater treatment systems has also been reported. For instance, one annual survey based on monthly data of concentrations of engineered ZnO nanoparticles in a wastewater treatment plant in the USA reported the inflow concentration of ZnO nanoparticles in the 20.0 ± 12.0–212.0 ± 53.0 μg/L range (Choi et al., 2018). The amounts of ZnO nanoparticles fran captured by sludge particulates were, according to the yearly average, 7.1 kg-ZnO/day, and 8.9 kg-ZnO/day, for the primary and secondary sludge particulates, respectively (Choi et al., 2018). Zinc element concentrates in the environmental waters, sediments and organisms in two forms, i.e. ZnO nanoparticles and ionic forms. The different forms have completely different characteristics related to their water persistence. Intrinsically, the zinc ions are persistent, but they can also convert into secondary species leading to the formation of some complex compounds such as zinc hydroxide and chloro complexes. They do this by interacting with substances/chemicals present in the environmental and seawaters. On the other hand, ZnO nanoparticles can dissolve and form aggregates by losing their parental characteristics to generate complex compounds (Yung et al., 2014). The dissolution of ZnO nanoparticles depends on the pH of the media. Dissolution of ZnO nanoparticles is faster in the acidic medium and lower dissolution occurs at basic pH (Cardoso et al., 2022, 2021).

Moreover, the presence of ZnO nanoparticles in the environment could be toxic to the environment, flora and fauna (Rajput et al., 2018). It is reported that a marine diatom known as *Phaeodactylum tricornutum* was shown to be less sensitive to ZnO nanoparticles compared to another diatom known as *Thalassiosira pseudonana* (Peng et al., 2011). A decline in the cell division of *T. pseudonana* was observed and it was suggested this occurred due to the disturbance of silicon uptake and the formation of frustule in the dissolved zinc ions derived from the ZnO nanoparticles (Peng et al., 2011).

Zinc oxide nanoparticles could also interact with, each other (particle-particle interactions), co-existing natural and synthetic compounds present in the environmental waters including electrolytes, and surface of the media (deposition/particle-surface interactions) to create complex substances (Bhattacharjee et al., 2000; Gomez-Flores et al., 2020; Khan et al., 2023; Liu et al., 2010; Ma et al., 2020). The particles shape and orientation also influence on their transport behaviour and stability in the porous media and their deposition under the various ionic strength (Gomez-Flores et al., 2020; Liu et al., 2010). For instance, less straining of rod-shape particles compared with spherical ones in saturated porous media were reported demonstrating that the minor axis was the critical dimension directing the whole process. An instantaneous release of spherical particles on elution was reported, however the release of rod-type particles was rate limited, indicating the effect of orientation for rod-type colloids (Liu et al., 2010).

Environmental determinants such as pH, temperature, salts, and the presence of other artificial (organic compounds such as flame retardants) and natural (humic and fulvic) substances may also shape the interactions of ZnO nanoparticles in water systems (Bhatt and Tripathi, 2011; Khan et al., 2023). For example, one study on the interaction between ZnO nanoparticles and α-linolenic acid and bovine serum albumin-complexed α-linolenic acid reported the presence of these substances (α-linolenic acid and bovine serum albumin-complexed α-linolenic acid) could change the hydrodynamic sizes, surface charge, and fluorescence of nanoparticles due to coating effects (Zhou et al., 2017).

Similarly, the interaction mechanisms of organic pollutant (hexabromocyclododecane) and ZnO nanoparticles with aging factor under various environmental conditions have been reported by Khan et al. (2021). Aggregation behaviour of the nanoparticles was observed in the presence of hexabromocyclododecane and salts with the passage of time affecting the size, shape, crystallinity and electrical charge of nanoparticles. However, comparative dispersion behaviour of nanoparticles was also observed with their humic acid interactions (Khan et al., 2021). Similarly, the fate and behaviours of ZnO nanoparticles in the presence of brominated flame retardants (polybrominated diphenyl ethers) as organic pollutants in the water systems were reported (Khan et al., 2019).

To explain the influence of ZnO nanoparticles in wastewaters and their behaviour, it is necessary to investigate the primary features of their interactions with other co-existing materials. Studies revealed the impacts of nanoparticles on biological wastewater treatment and sludge digestion by employing toxic effects on bacteria present in activated sludge and/or anaerobic granular sludge process (Joo and Aggarwal, 2018; Selck et al., 2016; Wang and Chen, 2016). Usually, such studies were conducted employing synthetic wastewater samples, which caused many challenges when the same conclusions were applied to real wastewater samples. Scientists began to investigate the impact of nanoparticles on samples collected from actual wastewater treatment plants, and found different outcomes compared to those using synthetic wastewaters (Zheng et al., 2019). Real wastewater samples contain more dissolved natural and/or synthetic organic compounds including salts compared to synthetic ones. The presence of such substances may impact and alter the behaviour of (ZnO) nanoparticles compared to synthesized wastewaters (Zhang et al., 2009; Zheng et al., 2019).

The importance of the physicochemical characteristics is in the Derjaguin-Landau-Verwey-Overbeak (DLVO) theory for assessing the stability and deposition of the nanoparticles in the environmental media. Unique configurations of synthesised nanoparticles and their suspensions are being generated by manipulating the characteristics of the nanoparticles such as size, shape, structure, surface coatings and chemical composition. Although these characteristics make nanoparticles more promising for new applications, but in parallel, they also challenge to understand nanoparticles aggregation in the environmental media and the consequent effects on their transport and interactions with environmental existing co-contaminants. Nanoparticles accumulation and deposition in the environmental media indicate their

transport potential, environmental fate and behaviour, and influential eco-toxicological effects (Hotze et al., 2010; Petosa et al., 2010; Tufenkji and Elimelech, 2004; Yotsumoto and Yoon, 1993).

This study aims to identify the real physicochemical characteristics of ZnO nanoparticles from household sunscreen to real wastewaters. Various ZnO-based sunscreens manufactured in Australia and elsewhere were purchased from a local market. Wastewater samples (influents and effluents) were collected from wastewater treatment plants. Extraction method was applied to extract ZnO nanoparticles from the purchased sunscreen samples (named as S1, S2, S3, and S4) and the real wastewater samples (named as WW1 to WW7). The characteristics of ZnO nanoparticles were compared with that purchased from Sigma-Aldrich. TiO_2 and Ag_2O nanoparticles including Fe fine powder were also characterised using TEM to make a comparison with the particles detected in the wastewaters. The findings revealed important ractifications from the assessment of exposure to ZnO nanoparticles and co-contaminants which are influenced by products and water conditions.

2. Materials and methods

2.1. Materials

Four commercial ZnO-based sunscreens produced around the world were purchased from a local market in Australia. The samples were labelled S1, S2, S3, and S4. Wastewater was sourced from New South Wales (NSW) Australia.

ZnO nanoparticles (particle size <100 nm), titanium (IV) oxide, $nTiO_2$ (particle size <25 nm, 99.7% trace metals basis), silver (I) oxide, Ag_2O (≥99.0 %), and iron (=99%, reduced fine powder) were sourced from Sigma-Aldrich®. Characteristics of ZnO nanoparticles used in this study have been reported in our previous research (Khan et al., 2021). Ethyl alcohol and tetrahydrofuran (THF) were purchased from Ajax Finechem, Thermo Fisher Scientific and Sigma-Aldrich®, respectively, and used as received. Formamide, and 1 bromonaphthalene were purchased from sigma-Aldrich® and used as received. Syringe filters (0.22 μm), syringes (1 mL) and centrifuge tubes (2 mL) were obtained from Fisher Scientific (Houston, TX, USA). Disposable folded capillary zeta cells (DTS1070) for dynamic light scattering were obtained from Malvern Instruments Ltd. in the UK. Copper grids (Lacey carbon film, 300 mesh) for TEM imaging were obtained from PST (ProSciTech), Australia.

2.2. Extraction of metal oxide nanoparticles from sunscreens and wastewaters

The THF (10 mL) was added to a conical flask containing the sunscreen sample (100 mg). The mixture was agitated overnight using a magnetic stirrer to completely disperse the nanoparticles. The dispersed sample was centrifuged at 18407 rcf (relative centrifugal force) for 45 min by using Eppendorf Centrifuge 5424. The supernatant was discarded, and the sediment was dispersed in 10 mL of ethanol to remove any solvent affiliated with the sediment (settled down particles). The ethanol dispersions were centrifuged by applying the same method mentioned above. The organic solvent removal procedure using ethanol was performed three times. The sediment (settled down nanoparticle) was dried naturally and stored for further analysis.

All raw wastewater samples were sonicated at 20 °C for 60 min in 50 mL centrifuge tubes full of wastewater. 10 mL wastewaters were filtered with polyether sulfone (PES, 0.22 μm) and placed in new same type of 50 mL centrifuge tubes. 10 mL water samples of each kind of wastewater were centrifuged at 18407 rcf for 60 min in the Eppendorf Centrifuge 5424. A portion of the supernatants were discarded, and the residue suspensions were stored and dropped on the TEM grids for further analysis.

2.3. Hydrodynamic size and zeta potential analysis

The purchased and extracted ZnO nanoparticles stock suspension was prepared by adding 0.1 g of ZnO nanoparticles to 1 L Milli-Q water. This was followed by sonication for 10 min. The pH (4, 7, and 10) of samples were maintained by using buffer solutions. The prepared suspensions were analysed using Malvern Panalytical Zetasizer at room temperature (i.e. 20 °C). The suspensions were analysed after 24 h for the characteristics to investigate the aging effect, i.e. 0 h (immediately after solution preparations) and 24 h (solutions were in a stationary status for 24 h, and simply hand-shaken prior to analysis).

2.4. Characterization techniques

Transmission electron microscopy (TEM), X-ray powder diffraction (XRD), Fourier transform infrared spectroscopy (FTIR), and Micromeritics TriStar II were used to characterise the nanoparticles. Inductively coupled plasma mass spectrometry (ICP-MS), and Inductively Coupled Plasma Optical Emission spectroscopy (ICP-OES) were used to determine the concentrations of dissolved metal ions in the wastewater samples (filtered by using polyether sulfone (PES, 0.22 μm) syringe filters), and to measure the dissolved zinc at various pH. Malvern Panalytical Zetasizer was employed to investigate the zeta potential and particle size of extracted particles. The contact angle of the nanoparticles pallets was measured on an OCA 20 tensiometer (Data-physics) for the determination of Hamaker constant (Ma et al., 2010). A 10 μL droplet (Milli-Q water, formamide, and 1 bromonaphthalene) was placed on the pallet and both left and right contact angle measurements were taken using the native instrument software (Lobel et al., 2022). The Hamaker constant representing the van der Waals (vdW) interactions were calculated using Zisman plot for the extracted nanoparticles (Supplementary information, Fig. S1).

3. Results and discussion

3.1. Morphological analysis of nanoparticles

TEM analyses were conducted for purchased ZnO nanoparticles and the nanoparticles extracted from the sunscreens. It was observed that the ZnO nanoparticles were rod and spherical in shape with particle sizes ≥ 100 nm but the majority of them were less than 100 nm (Fig. 1, ZnO (a-b)). A highly lattice pattern (Fig. 1, ZnO(c)) followed by bright spots in the diffraction pattern (Fig. 1, ZnO(d)) indicated the purity and crystallinity of the ZnO nanoparticles representing the same characteristics as we reported in our previous study (Khan et al., 2021). Elemental composition (Fig. S2) further confirmed the presence of zinc and oxygen atoms as was found in the ZnO nanoparticles. The presence of Carbon and Copper in the Energy dispersive X-ray (EDX) spectrum and the quantification table (Fig. S2) is from the Copper grid (Lacey carbon film, 300 mesh) used for TEM analysis.

TEM images of sunscreen 1 (S1) revealed that ZnO nanoparticles used in the S1 were very distinct and diverse. Particles had three shapes, which were irregular, spherical and elongated. The nanoparticles were less than 100 nm in size and the majority were smaller than 50 nm (Figs. 1, S1(a, b)). Higher magnification resolution and diffraction further explained the high lattice pattern (Figs. 1, S1(c)) and crystallinity (Figs. 1, S1(d)) of the particles. Only one shape (spherical) of particles was found in sunscreen 2 (S2) having a size smaller than 50 nm (Figs. 1, S2). Aggregation behaviour of the ZnO nanoparticles in S2 could be due to the small size of nanoparticles that tend to gather because of van der Waals forces, electrostatic and hydrophobic interactions. This was even after the S2 nanoparticles had been dispersed in ethanol followed by bath sonication for 15 min prior to being placed on a TEM grid. A similar agglomeration pattern was noted in Fig. 1, (S1 and Sigma-Aldrich ZnO nanoparticles). Bright spots representing the crystalline nature of the nanoparticles was also observed (Fig. 1, S2(c,

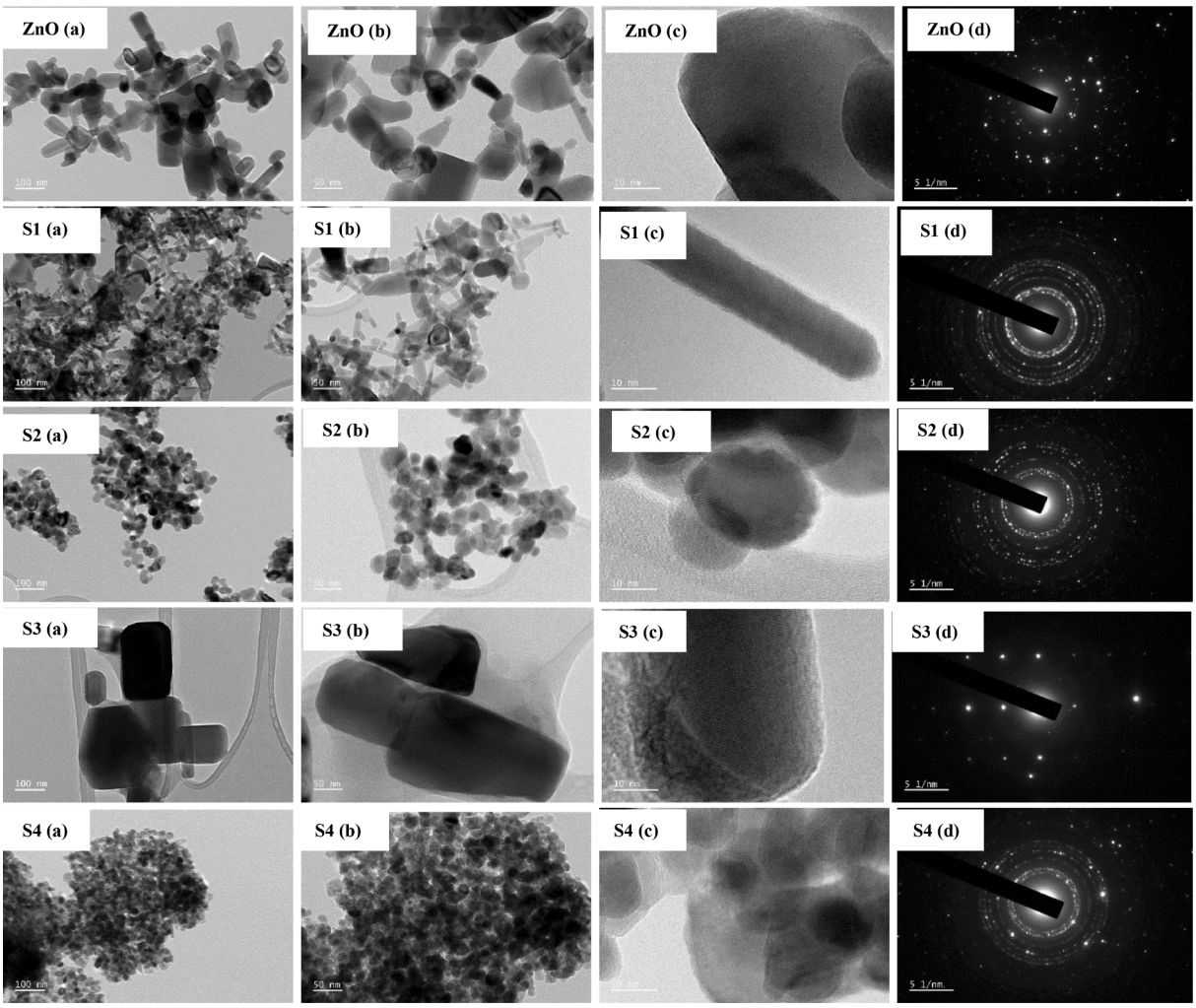

Fig. 1. TEM analysis of ZnO nanoparticles (Sigma-Aldrich) and the nanoparticles extracted from the sunscreens. The scale bars from left to right are 100 nm, 50 nm, 10 nm and 1 nm, respectively.

d)). A different pattern in the particle size and shape of ZnO nanoparticles was observed in sunscreen 3 (S3) (Figs. 1, S3). It was noted that the majority of particles were larger than 100 nm and composed of rectangular and spherical shapes (Figs. 1, S3 (a, b)) with less aggregation compared to all other particles. The level of crystallinity of S3 particles could be observed (Figs. 1, S3(c, d)). Sunscreen 4 (S4) particles had the same shape as S2 with the particles being smaller than S2 which led to agglomeration. They were also highly crystalline (Figs. 1, S4 (c, d)). Energy dispersive X-ray spectroscopy analysis confirmed the presence of zinc and oxygen in all sunscreens nanoparticles (Fig. S2). However, a minor quantity (mass %) of Silica (Si) were observed in sunscreens S1, S2, and S4 (Fig. S2) which could be due to some remaining substances present in the sunscreens and could not be removed completely during extraction process. The presence of Carbon and Copper in the Energy dispersive X-ray (EDX) spectrum and the quantification table (Fig. S2) is from the Copper grid (Lacey carbon film, 300 mesh) used for TEM analysis.

Virtually all the ZnO nanoparticles in all sunscreens samples as well as Sigma-Aldrich ZnO nanoparticles were aggregated. Less agglomeration was observed in S3 nanoparticles. However, based on this observation, we could assume that the size of the particles matters to some extent as influencing the aggregation behaviour of the nanoparticles. Homo-agglomeration (particle-particle interactions)/aggregation of the nanoparticles usually occurs and could be instantaneous if nanoparticles are present in the solvent/solution. They form the agglomerate/aggregate sizes in $\geq$ 100 nm due to a combination of van der Waals forces including electrostatic, and hydrophobic interactions (Bathi et al., 2021; Lead et al., 2018) as observed in Fig. 1. This also agrees with the Hamaker constant determined from contact angle measurement and using Zisman plot as S3 showed the lowest value.

Alterations in the morphological behaviour affecting the fate of the nanoparticles could be assumed once they are released into waters, depending on the associated co-contaminants under various conditions. Both steric and charge repulsion were reported in studies on the behaviours of nanoparticles in the presence of natural organic substances which helped nanoparticles stabilise against agglomeration (Lead et al., 2018; Yang et al., 2017). The total organic carbon (TOC, mg/L) measurements were performed to confirm the presence of any left over associated organic substances with the extracted nanoparticles (such as S1, S2, S3, and S4) at various controlled pH (4, 7, and 10). The results revealed most of the samples contain below LOR for TOC (1 mg/L) with only S1 indicated 2-3 mg/L TOC in the solution. The results suggested the extraction procedure removed the excessive associated organic carbons to obtain the nanoparticles.

Similarly the aggregation behaviour of nanoparticles in the presence of electrolytes especially salt-type ones and their ionic strength was observed due to more electrical conductivity, accumulation of charged particles by compressing the electrostatic double layers and a decline in repulsive forces (Bathi et al., 2021). Similar findings for the Sigma-Aldrich ZnO nanoparticles in the presence of humic acid and

electrolytes were noted (Khan et al., 2021).

3.2. Mineralogical, surface functional groups and porosity analysis of nanoparticles

The X-ray diffraction analysis of purchased ZnO nanoparticles and those extracted from the sunscreens is shown in Fig. 2(a). Sharp peaks at 2 thetas (θ) value 31.9°, 34.6°, and 36.9° for ZnO nanoparticles representing the crystal (hexagonal wurtzite) structure of the nanoparticles with three perfect alignments - (1 0 0), (0 0 2) and (1 0 1). These alignments match with the defined standard powder diffraction (JCPDS, No. 36-1451) (Khan et al., 2021; Zak et al., 2011). It was observed that samples from S1 to S4 followed the characteristics peaks of ZnO nanoparticles.

FTIR analysis (Fig. 2(b)) revealed the presence of Zn−O binding in the samples extracted from the sunscreens. Peaks at 430 cm^{-1} were observed in all samples as Zn−O was present between the range for metal oxides, i.e. 400–600 cm^{-1} (Chandrasekar et al., 2021; Gharagozlou and Naghibi, 2016; Khan et al., 2021). A peak at 1095 cm^{-1} was only observed in S1 which could be due to Silica which has also been detected in S1 in EDX spectrum (Fig. S2). It could be assumed that a few traces of silica substances could remain attached to the S1 nanoparticles, even after extraction. Although some mass fractions of Silica has also been detected in Sunscreens S2 and S4 but the mass% of Silica is very less in these samples compared to detected in S1 (Fig. S2-EDX spectrum and quantitative table). The peaks at 2360 cm^{-1} could be due to carbon dioxide from the atmosphere and 2920 cm^{-1} could be due to stretching followed by bending motion of C–H caused by a few remaining associated organic molecules (Ham et al., 2015; Stuart, 2004). The peak at 3440 cm^{-1} reflected OH stretching. It is likely due to moisture, but it may also be due to surface OH groups as ZnO will likely have some OH groups on the surface (Khan et al., 2021; Stuart, 2004; Zak et al., 2011). In sample S4, a small peak at 1800 cm^{-1} is due to C=O stretching which may have been caused by trace amounts of associated organic molecules present in the S4 sample.

Based on FTIR analysis, two common peaks at 430 and 3440 cm^{-1} in all samples explained the presence of zinc/oxygen and moisture contents (O−H) from the atmosphere respectively. However, all extracted samples from S1 to S4 indicated slight differences due to the presence of associated organic molecules. Here the associated elements in S2 and S3 are virtually the same, but a few extra different peaks were identified in S1 and S4 (Fig. 2b). FTIR analysis showed that the extracted samples (ZnO nanoparticles) are very similar to ZnO nanoparticles purchased from Sigma-Aldrich, with some attached organic substances (which have also observed from the TOC measurements) in the extracted samples.

The adsorption isotherms and surface area analysis of purchased ZnO nanoparticles indicated the BET and Langmuir surface areas were 12.26 and 27.51 m^2/g with an average particle size of 94.96 nm (Khan et al., 2021). Similar results were observed for nanoparticles extracted from the sunscreens except for S3. For instance, the BET and Langmuir surface areas of S1 were 12.64 and 23.17 m^2/g, S2 were 11.16 and 20.12 m^2/g, S3 were 0.59 and 0.81 m^2/g, and S4 were 17.90 and 46.21 m^2/g, respectively. The average particle sizes for S1, S2, S3, and S4 were

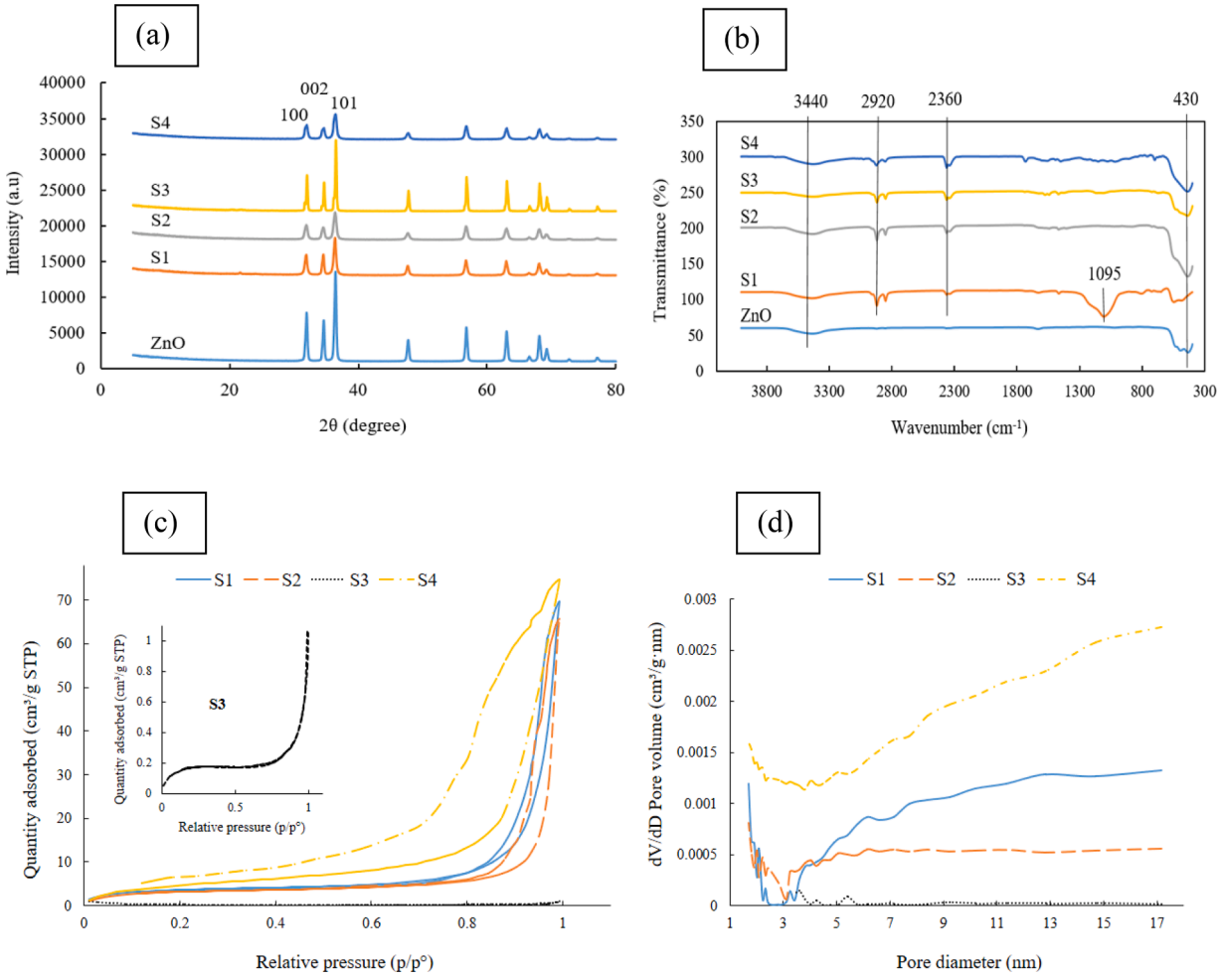

Fig. 2. Mineralogical and adsorption analysis of purchased and extracted ZnO nanoparticles, XRD pattern (a), FTIR (b), adsorption isotherms (c), and first derivative of pore volume versus pore diameter (nm) (d).

474.8, 537.7, 10197.6, and 335.2 nm, respectively. The smaller surface area and large average particle size of S3 are consistent with results of the TEM analysis (Fig. 1, S3 (a-b)).

The type IV isotherms (Fig. 2c) were observed for S1, S2, and S4 which revealed that the hysteresis loops were unusually associated with the filling and emptying of the mesopores of ZnO nanoparticles by capillary condensation (Rouquerol et al., 1999). However, S3 followed the type II isotherm pattern and represented macro-porous or non-porous adsorbent (Fig. 2c) leading to less gas being adsorbed for S3. Fig. 2d depicted the first derivative of pore volume versus its pore diameter (nm). It was observed that the distribution representations of S1, S2, and S4 were bimodal pore size which is usually the case in the mesoporous region (2–15 nm), where a significant mesoporous structure of S1, S2, and S4 extracted ZnO nanoparticles is evident (Khan et al., 2021; Liu et al., 2015). Conversely, a virtually linear line could be observed for S3 (Fig. 2d) and this indicates macro-porous/non-porous ZnO nanoparticles as confirmed by TEM analysis (Figs. 1, S3 (a, b)). The ZnO nanoparticles in S3 were slightly larger compared to other purchased and extracted varieties.

3.3. Particle size and surface charge analysis

The hydrodynamic size of purchased and extracted ZnO nanoparticles was determined at pH 7 (controlled by using pH 7-Phosphate buffer solution) at room temperature (20 °C) after 0 h and 24 h interactions in Milli-Q water (Fig. 3(a, c)). After 0 h, the particle size range of purchased ZnO nanoparticles was 106−1190 nm (Fig. 3a). Similarly, the size ranges of S1, S2, S3, and S4 were 122−531 nm, 106−955 nm, 142−1110 nm, and 255−825 nm, respectively (Fig. 3a). Increase in the size ranges were observed after 24 h interactions (Fig. 3b). For instance, the size range of purchased ZnO nanoparticles was 142−2670 nm. The same observations were measured for extracted ZnO nanoparticles (Fig. 3b). The overall increase in the hydrodynamic size of nanoparticles could be due to aggregations of nanoparticles caused by van der Waals forces, hydrophobic and electrostatic interactions in aqueous media. This was also consistent with findings normally observed in the behaviour of purchased and extracted nanoparticles analysed by TEM (Fig. 1) (Bathi et al., 2021; Bhatt and Tripathi, 2011; Khan et al., 2023; Lead et al., 2018). Fig. 3c depicted the particle size of nanoparticles at the peak of the particle size distribution curve (PSDC) which was represented as “particle size at peak of PSDC (d, nm)”. It was observed that after 24 h the size of the nanoparticles at PSDC increased compared to 0 h interactions. More agglomeration effects were observed in all nanoparticles compared to 0 h which could be due to particle-particle interactions, van der Waals forces (Hamaker constant), hydrophobic interactions.

The surface charge analyser measured an overall charge (−45.9 mV) on the surface of purchased ZnO nanoparticles, which altered to −43.8 mV after 24 h interactions. This was due to aggregation that covered some active sides of the nanoparticles. Similar trends were observed in the extracted nanoparticles after 0 and 24 h interactions. For instance, the electrical potential of S1, S2, S3, and S4 dropped in magnitude from −12.1, −12.0, −12.4, and −21.1 mV (0 h) to −6.2, −5.7, −8.2, and −13.4 mV (24 h), respectively (Fig. 3d). The agglomeration effect with aging factors was reported (Khan et al., 2021). It was observed that the surface charge of the nanoparticles was diminished markedly after 24 h interactions. This may be linked to the agglomeration and aggregation behaviour of nanoparticles in terms of sedimentation. However, it was observed that the magnitude of the surface charge was higher in S4, which would have a lower aggregation potential. Furthermore, these magnitudes are very low and one would expect the aggregation of these particles.

To further confirm this behaviour of extracted nanoparticles, the surface charge and size of the particles such as ZnO nanoparticles and extracted ones were again analysed (new batch of samples were prepared) at various controlled pH such as 4, 7, and 10 to examine the surface charge and aggregation trends. The overall surface charge and aggregation trends of all the particles remained same (Figs. S3, S4, and S5). However some variations in the surface charge and size values could be observed in extracted nanopartciles behaviours by comparing Fig. 3 to (Figs. S3, S4, and S5) because of unequal suspension of each extracted nanoparticles compared to purchased ZnO nanoparticles (surface charge and size values trends of purchased nanoparticles were remained the same). At lower pH (pH 4), the magnitude of the surface charge values of

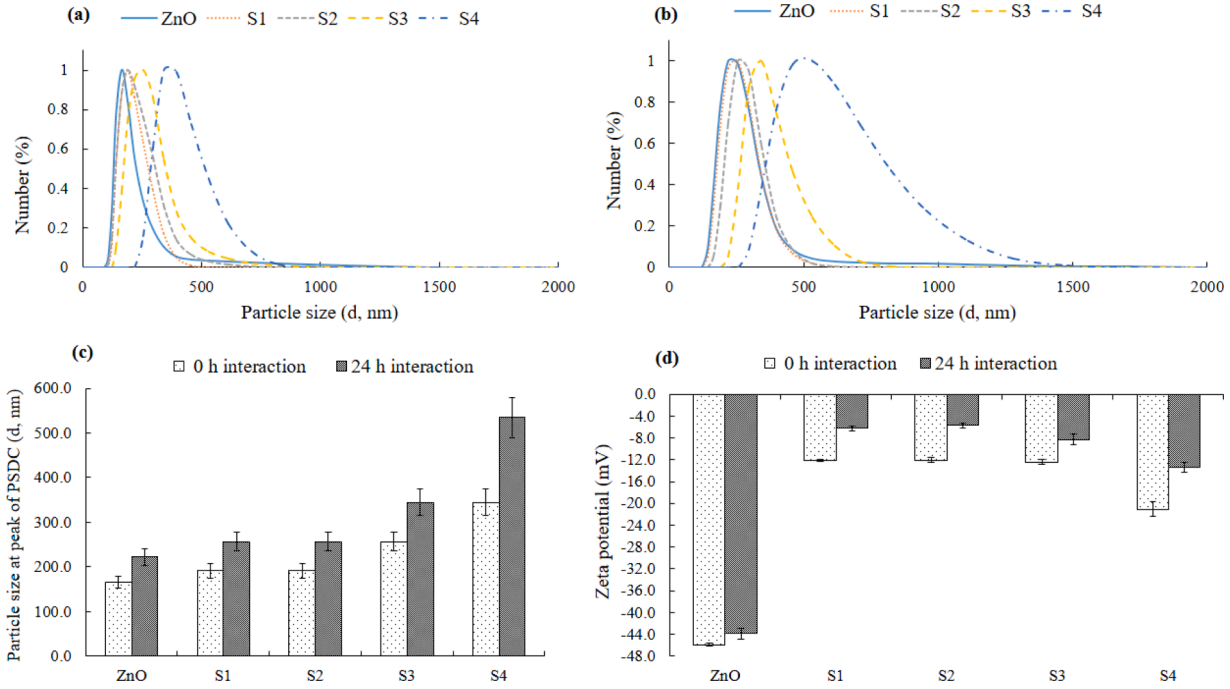

Fig. 3. Particle size distributions after 0 h interactions (a), 24 h interactions (b), particle size at peak of PSDC after 0 and 24 h interactions (c) and surface charge analysis (d) of purchased and extracted ZnO nanoparticles at pH 7 under room temperature 20 °C.

all nanoparticles were low however the magnitude of the surface charge increased (become more negative) at higher pH (such as pH 7, and pH 10).

Once the metal oxides are in the water, development of hydroxide layers (≡M-OH) on the surface of metal oxides due to hydrolysis is a common process, as water molecules can be adsorbed (both chemically and physically) onto the surface of the particles (dispersed oxides). However, the hydroxide layers developed charged by reacting with positively charged (H^+) and/or negative charged (OH^-) species due to surface amphoteric reactions altering the surface charge values at low pH (by adsorption of proton H^+) and higher pH (losses of proton) (Blok and Bruyn, 1970). Similarly in this study the magnitude of the surface charge values are high (more negative) at higher pH (such as pH 10) and magnitude of the surface charge values are low (less negative) at low pH (such as 4). The alterations in the size distribution of the nanoparticles at various pH with aging factor (after 24 h) has also been observed (Figs. S4, and S5). For instance, the particle size distributions and the size at peak of particle size distribution curve (PSDC) also increased compared to 0 h as pH increased from lower (pH 4) to higher (pH 10). The increase in the size of nanoparticles at higher pH after 24 h could be due to the adsorption of hydroxyls onto the hydroxide amphoteric surface (nanoparticles sites) and/or the development of hydroxylated zinc

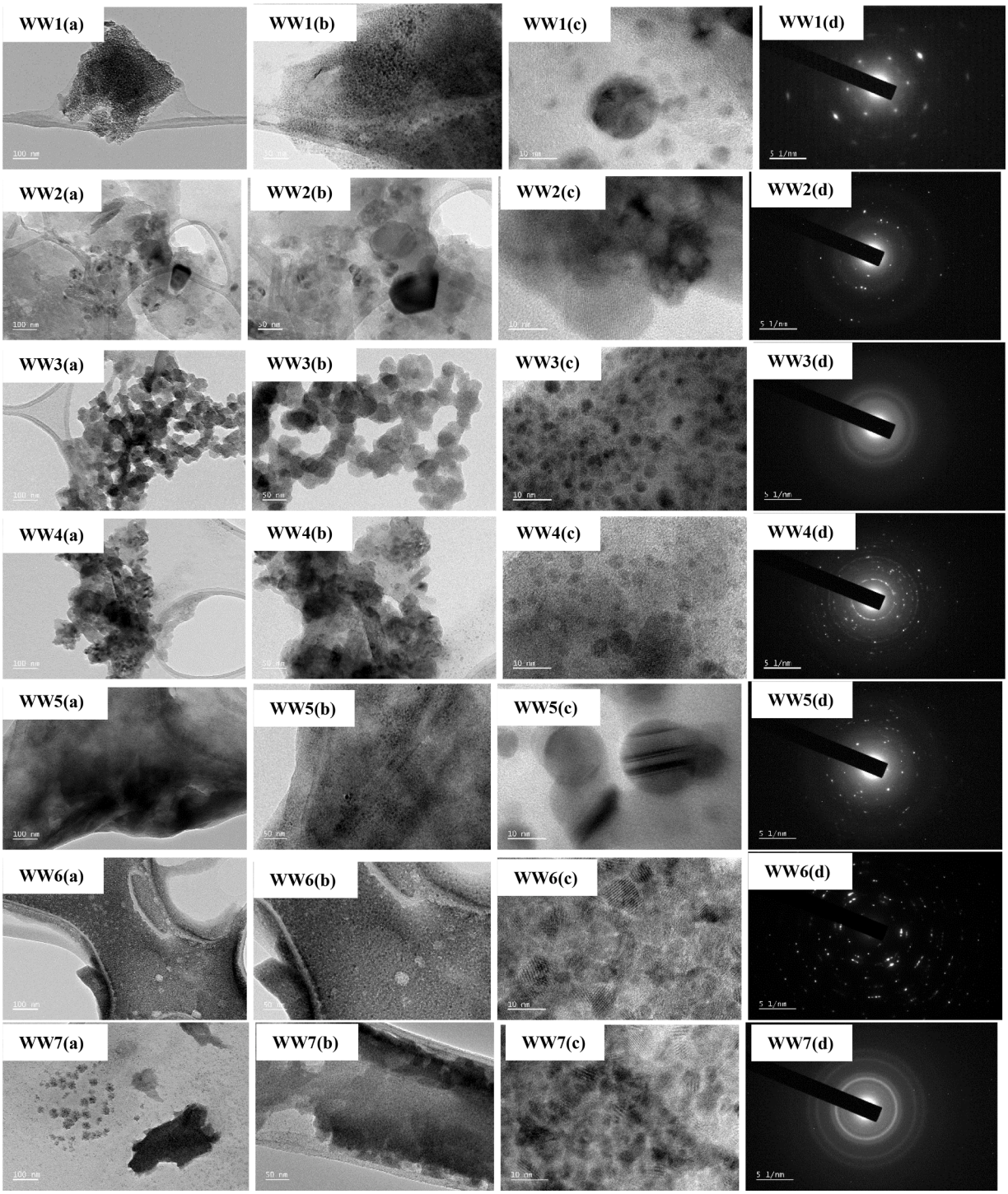

Fig. 4. TEM images of wastewater samples, where WW1, 2, 3 and 7 represent influents and WW4, 5 and 6 are effluents.

species, based to the following reactions;

$$Zn_{(aq)}^{2+} + OH_{(aq)}^{-} \leftrightarrow Zn(OH)_{(aq)}^{+}$$

$$Zn(OH)_{(aq)}^{2+} + OH_{(aq)}^{-} \leftrightarrow Zn(OH)_{2s}$$

$$Zn(OH)_{2s} \leftrightarrow Zn(OH)_{2(aq)}$$

The dissolution behaviour of ZnO nanoparticles extracted ones were determined (Fig. S6). It depicted that at lower pH 4 (acidic conditions) the concentrations (mg/L) of dissolved zinc of all nanoparticles are high due to high dissolution of nanoparticles in Milli-Q water due to attach of protons on the surface of the nanoparticles. The soluble ionic forms of dissolved nanoparticles could be due to $Zn_{(aq)}^{2+}$ ions at lower pH. Less dissolution was observed for all nanoparticles at higher pH (Fig. S6) which could be associated due to the formation of the hydroxide compounds (Bian et al., 2011).

3.4. Occurrence of nanoparticles in wastewater samples

Trace amounts of heavy metals, specifically Beryllium (Be), Chromium (Cr), Iron (Fe), Manganese (Mn), Cobalt (Co), Nickel (Ni), Copper (Cu), Zinc (Zn), Arsenic (As), Selenium (Se), Cadmium (Cd), and Lead (Pb) were analysed in the wastewater samples. Tabular concentrations of heavy metal elements are presented in Table S2. According to the World Health Organization, the acceptable limits of some heavy metal ions in drinking water are as follows: Pb (50 μg/L), Cd (5 μg/L), Cr (50 μg/L), Zn (5000 μg/L), Cu (1500 μg/L), Co (10 μg/L), and Ni (100 μg/L) (Ekramul Mahmud et al., 2016). According to Australian drinking water guidelines 2011, version 3.4 updated October 2017, based on human health considerations the concentrations of antimony, arsenic, Beryllium, Cadmium, Chromium, Copper and Nickel, in drinking waters should not exceed 3, 10, 60, 2, 50, 1000, and 20 μg/L, respectively (NHMRC; NRMMC, 2011). However, wastewater treatment works are typically bound by licence conditions with specific concentration limits for various metals, and the limits may vary depending on the sensitivity of the receiving environment.

TEM analysis was performed to further confirm the shape, size and detection of metal-based nanoparticles. The TEM images of wastewater samples (Fig. 4) and their elemental compositions with mapping (Fig. S7 (a–g) were documented. Various shapes of nanoparticles with different sizes and other dissolved substances were detected in samples. For instance, in Fig. 4 WW1(a, b), highly dense and thick contaminant concentrations prevent electron beams passing through where a lot of nanoparticles, mostly less than 50 nm, were also observed. Particle size $\leq$ 10 nm with lattice pattern can be seen in Fig. 4 WW1c. A diffraction image (Fig. 4 WW1d) with bright spots further confirmed the presence of highly crystalline (lattice) particles present in this waste sample. Elemental compositional mapping (Fig. S7a) explained the presence of trace amounts of other elements including Ag, Br, Cl, F, Fe, Ti, Zn, and O.

The WW2 contained small, irregular, and spherical nanoparticles that were less than 100 nm (Fig. 4 WW2 (a, b)). A high lattice pattern and bright spots in the diffraction image can also be observed in Fig. 4 WW2 (c, d)). The elemental composition further confirmed the presence of metal elements such as Al, Fe, Mg, Ni, Ti, and Zn with other compounds containing F, Cl, and S, etc. (Fig. S7b).

The shape and size of particles in the WW3 sample (Fig. 4 WW3(a, b)) were similar to particles extracted from sunscreens S2 and S4 (Fig. 1 S2 (a, b) and S4(a, b)). However, these particles (WW3) were less crystalline compared to that found in the other samples. It was observed that the particles closely interact with other organic and/or inorganic substances such as Br, Cl, F, P, S, Si, Ti, Zn, and O and salts (Ca/Na) (Fig. S7c). Spherical and rod-shapes with highly packed and interacted nanoparticles were observed in WW4 (Fig. 4 WW4(a-b)). A very intricate lattice pattern with bright spots due to high crystallinity was observed in the WW4 sample (Fig. 4 WW4(c-d)). Elemental mapping revealed the presence of Ag, Al, Br, C, Ca, Cd, Cl, F, Fe, K, Mg, Na, Ni, O, P, S, Si, Ti, and Zn (Fig. S7d). Contaminants including nanoparticles in WW5 were like those found in WW1 followed by the lattice patterns with similar elements discovered in elemental mapping (Figure S7e). Compacted morphology was observed in the WW6 and WW7 samples where the nanoparticles appeared to be crossed-linked and interacted with other organic and inorganic substances (Fig. 4 WW6-7(a-b)). High resolution and diffraction images exhibited the high lattice and crystalline surface of the nanoparticles ($\leq$10 nm) present in wastewater samples. Various organic and inorganic elements were detected in these samples and their mapping is illustrated in Figure S7(f-g)).

To better understand the types of nanoparticles detected in the wastewater samples, the TEM analyses of TiO_2 nanoparticles, Ag_2O nanoparticles, and Fe-powder purchased from Sigma-Aldrich were conducted (Figure S8 and Figure S9). The results of TEM images of wastewater samples were compared with the TEM images obtained for these nanoparticles and ZnO nanoparticles extracted from sunscreen samples and purchased from Sigma-Aldrich (Fig. 1). Rod and spherical crystalline shape of TiO_2 were observed with the majority of particles less than 100 nm in size (Fig. S8 (a–d)). A similar shape was observed in the particles detected in WW2(a, b) and WW4(a-b) (Fig. 4). It could be assumed that WW2 and WW4 are accumulated with TiO_2 nanoparticles entering the community wastewaters due to the use of personal care products, paints and coatings, etc., which generally end up in bodies of water (Reyes-Herrera et al., 2022). The presence of titanium has also been detected in all samples during mapping.

Similarly, Ag_2O nanoparticles are overall less than 100 nm in size with the majority of particles having a spherical shape with a high lattice-like surface morphology (Fig. S8 Ag_2O (a–d)). Almost the same particle size, shape and crystallinity were detected in the WW1, 4, and 7 samples and silver (Ag) has been observed in the elemental mapping (Fig. S7a, S7d, and S7g). The purchased iron powder particles were highly agglomerated, and their size and crystallinity were depicted in the TEM images (Fig. S8, Fe(a–d)). The presence of iron element is evident in all wastewater samples, which means traces of iron element may be originated from people's daily activities and then pass through the sewerage pipelines.

Zinc and oxygen were detected virtually in all samples and this constitutes evidence for the presence of ZnO nanoparticles. For instance, in comparison with the TEM images for ZnO nanoparticles purchased from Sigma-Aldrich and the ones extracted from sunscreen, the ZnO nanoparticles identified in Fig. 4 WW1(c), WW2 (a–c), WW3 (a–c), WW4 (a–c) are mostly spherical. Zinc was detected by elemental mapping in the other wastewater samples but it was difficult to observe the exact spherical shape of nanoparticles compared to Sigma-Aldrich purchased ZnO nanoparticles. This was due to them being highly packed and cross-linked with co-contaminants.

Significant alterations in the behaviour of nanoparticles were observed in terms of their purity, shape and charge based on a comparison of TEM analysis for ZnO nanoparticles purchased, extracted and those identified in wastewater samples. Agglomerations due to the presence of co-occurring organic and inorganic substances could also dictate the fate and behaviour of nanoparticles, mostly depending on environmental factors such as pH, temperature, salinity and their strengths.

4. Conclusions

Zinc oxide-based sunscreens contain particles with their measured size in nanometres. Four commercial sunscreens tested in this study contained nanoparticles ($\leq$100 nm in size, some particles $\geq$ 100 nm in S3). The nanoparticles extracted from the sunscreens had various shapes, aspect ratios, and wide-size distributions. Aggregation in the behaviour of all nanoparticles was observed with time intervals when checking their particle size and surface charge. The presence of nanoparticles in real wastewater samples was also characterised and compared with that in the extracted and purchased samples.

Comparison revealed that the nanoparticles in wastewater samples were mostly composed of zinc, titanium, and silver elements followed by iron particles and co-contaminants with other existing organic substances. This study demonstrated the different morphologies of nanoparticles extracted from sunscreens and wastewaters. The alterations in morphology, shape, size of nanoparticles after interactions with co-existing substances from wastewaters/seawaters/surfacewaters could potentially alter their adverse impact on aquatic organisms, which could be different from that derived using fresh nanoparticles.

CRediT authorship contribution statement

Anwar Ul Haq Khan: Methodology, Formal analysis, Writing – original draft. **Yanju Liu:** Supervision, Conceptualization, Visualization, Writing – review & editing. **Cheng Fang:** Supervision, Writing – review & editing. **Ravi Naidu:** Supervision, Funding acquisition, Writing – review & editing. **Ho Kyong Shon:** Supervision, Writing – review & editing. **Zoe Rogers:** Resources, Writing – review & editing. **Rajarathnam Dharmarajan:** Supervision, Writing – review & editing.

Declaration of Competing Interest

The authors declare that they have no known competing financial interests or personal relationships that could have appeared to influence the work reported in this paper.

Data availability

Data will be made available on request.

Acknowledgments

The first author acknowledges The University of Newcastle (UON), Australia, for granting the fully funded PhD (ECRHDR UNRS Central and UNIPRS) scholarship. The authors are grateful to crcCARE and GCER, UON Callaghan, NSW 2308, Australia, for providing financial assistance and research facilities to accomplish the tasks in this study. Authors also acknowledge the support of Professor Graeme Jameson, Miss. Kitty Tang, and Mr. Lonn Cooper from the Centre for Multiphase Processes, UON, for providing the facilities and training to conduct nanoparticles' size and surface analysis. Authors are grateful to Dr. Huiming Zhang from the EMX (Electron Microscope and X-ray) unit, UON, for providing the training and the TEM analysis facilities. Authors are grateful to Prof Erica Wanless and Mr Hayden Robertson from School of Environmental and Life Sciences for the support in contact angle measurement.

Supplementary materials

Supplementary material associated with this article can be found, in the online version, at doi:10.1016/j.envadv.2023.100381.

References

Adler, B.L., DeLeo, V.A., 2020. Sunscreen safety: a review of recent studies on humans and the environment. Curr. Dermatol. Rep. 9, 1–9. https://doi.org/10.1007/s13671-020-00284-4.

Attia, H., Nounou, H., Shalaby, M., 2018. Zinc oxide nanoparticles induced oxidative DNA damage, inflammation and apoptosis in rat's brain after oral exposure. Toxics 6, 1–20. https://doi.org/10.3390/toxics6020029.

Bairi, V.G., Lim, J.H., Fong, A., Linder, S.W., 2017. Size characterization of metal oxide nanoparticles in commercial sunscreen products. J. Nanoparticle Res. 19, 256. https://doi.org/10.1007/s11051-017-3929-0.

Bathi, J.R., Moazeni, F., Upadhyayula, V.K.K., Chowdhury, I., Palchoudhury, S., Potts, G. E., Gadhamshetty, V., 2021. Behavior of engineered nanoparticles in aquatic environmental samples: Current status and challenges. Sci. Total Environ. 793, 148560 https://doi.org/10.1016/j.scitotenv.2021.148560.

Bhatt, I., Tripathi, B.N., 2011. Interaction of engineered nanoparticles with various components of the environment and possible strategies for their risk assessment. Chemosphere 82, 308–317. https://doi.org/10.1016/j.chemosphere.2010.10.011.

Bhattacharjee, S., Chen, J.Y., Elimelech, M., 2000. DLVO interaction energy between spheroidal particles and a flat surface. Colloids Surf. A Physicochem. Eng. Asp. 165, 143–156. https://doi.org/10.1016/S0927-7757(99)00448-3.

Bian, S.W., Mudunkotuwa, I.A., Rupasinghe, T., Grassian, V.H., 2011. Aggregation and dissolution of 4 nm ZnO nanoparticles in aqueous environments: Influence of pH, ionic strength, size, and adsorption of humic acid. Langmuir 27, 6059–6068. https://doi.org/10.1021/la200570n.

Blok, L., Bruyn, P.L.D., 1970. The ionic double layer at the ZnO solution interface. I. The experimental point of zero charge. J. Colloid Interface Sci. 32, 518–526. https://doi.org/10.1016/0021-9797(70)90141-4.

Cardoso, D., Narcy, A., Durosoy, S., Bordes, C., Chevalier, Y., 2021. Dissolution kinetics of zinc oxide and its relationship with physicochemical characteristics. Powder Technol. 378, 746–759. https://doi.org/10.1016/j.powtec.2020.10.049.

Cardoso, D., Narcy, A., Durosoy, S., Chevalier, Y., 2022. The pH dependence of dissolution kinetics of zinc oxide. Colloids Surf. A Physicochem. Eng. Asp. 650, 1–9. https://doi.org/10.1016/j.colsurfa.2022.129653.

Chandrasekar, M., Panimalar, S., Uthrakumar, R., Kumar, M., Saravanan, M.E.R., Gobi, G., Matheswaran, P., Inmozhi, C., Kaviyarasu, K., 2021. Preparation and characterization studies of pure and Li+ doped ZnO nanoparticles for optoelectronic applications. Mater. Today Proc. 36 (Pt.2), 228–231. https://doi.org/10.1016/j.matpr.2020.03.228.

Chatzigianni, M., Pavlou, P., Siamidi, A., Vlachou, M., Varvaresou, A., Papageorgiou, S., 2022. Environmental impacts due to the use of sunscreen products: a mini-review. Ecotoxicology 1331–1345. https://doi.org/10.1007/s10646-022-02592-w.

Chauque, E.F.C., Zvimba, J.N., Ngila, J.C., Musee, N., 2016. Fate, behaviour, and implications of ZnO nanoparticles in a simulated wastewater treatment plant. Water S.A 42, 72–81. https://doi.org/10.4314/wsa.v42i1.09.

Choi, S., Johnston, M., Wang, G.-S., Huang, C.P., 2018. A seasonal observation on the distribution of engineered nanoparticles in municipal wastewater treatment systems exemplified by TiO2 and ZnO. Sci. Total Environ. 625, 1321–1329. https://doi.org/10.1016/j.scitotenv.2017.12.326.

Cole, C., Shyr, T., Ou-Yang, H., 2016. Metal oxide sunscreens protect skin by absorption, not by reflection or scattering. Photodermatol. Photoimmunol. Photomed. 32, 5–10. https://doi.org/10.1111/phpp.12214.

Ekramul Mahmud, H.N.M., Obidul Huq, A.K., Yahya, R.B., 2016. The removal of heavy metal ions from wastewater/aqueous solution using polypyrrole-based adsorbents: a review. RSC Adv. 6, 14778–14791. https://doi.org/10.1039/c5ra24358k.

Gharagozlou, M., Naghibi, S., 2016. Sensitization of ZnO nanoparticle by vitamin B12: Investigation of microstructure, FTIR and optical properties. Mater. Res. Bull. 84, 71–78. https://doi.org/10.1016/j.materresbull.2016.07.029.

Gomez-Flores, A., Bradford, S.A., Hwang, G., Choi, S., Tong, M., Kim, H., 2020. Shape and orientation of bare silica particles influence their deposition under intermediate ionic strength: A study with QCM–D and DLVO theory. Colloids Surf. A Physicochem. Eng. Asp. 599, 124921 https://doi.org/10.1016/j.colsurfa.2020.124921.

Guedens, W.J., Reynders, M., Van Den Rul, H., Elen, K., Hardy, A., Van Bael, M.K., 2014. ZnO-based sunscreen: The perfect example to introduce nanoparticles in an undergraduate or high school chemistry lab. J. Chem. Educ. 91, 259–263. https://doi.org/10.1021/ed300851a.

Ham, W.S., Kim, M.K., Gim, J.S., Lee, J.S., Wu, J.H., Lee, K.B., Kim, Y.K., 2015. Microstructure and magnetic properties of LaSrMnO nanoparticles and their application to cardiac immunoassay. IEEE Trans. Magn. 51, 18–21. https://doi.org/10.1109/TMAG.2015.2438021.

Hotze, E.M., Phenrat, T., Lowry, G.V., 2010. Nanoparticle aggregation: challenges to understanding transport and reactivity in the environment. J. Environ. Qual. 39, 1909–1924. https://doi.org/10.2134/jeq2009.0462.

Hou, L., Xia, J., Li, K., Chen, J., Wu, X., Li, X., 2013. Removal of ZnO nanoparticles in simulated wastewater treatment processes and its effects on COD and NH4+-N reduction. Water Sci. Technol. 67, 254–260. https://doi.org/10.2166/wst.2012.530.

Joo, S.H., Aggarwal, S., 2018. Factors impacting the interactions of engineered nanoparticles with bacterial cells and biofilms: Mechanistic insights and state of knowledge. J. Environ. Manag. 225, 62–74. https://doi.org/10.1016/j.jenvman.2018.07.084.

Khan, A.U.H., Liu, Y., Naidu, R., Fang, C., Dharmarajan, R., Shon, H., 2021. Interactions between zinc oxide nanoparticles and hexabromocyclododecane in simulated waters. Environ. Technol. Innov. 24, 102078 https://doi.org/10.1016/j.eti.2021.102078.

Khan, A.U.H., Naidu, R., Dharmarajan, R., Fang, C., Shon, H., Dong, Z., Liu, Y., 2023. The interaction mechanisms of co-existing polybrominated diphenyl ethers and engineered nanoparticles in environmental waters : a critical review. J. Environ. Sci. 124, 227–252. https://doi.org/10.1016/j.jes.2021.10.018.

Khan, R., Inam, M.A., Khan, S., Park, D.R., Yeom, I.T., 2019. Interaction between persistent organic pollutants and ZnO NPs in synthetic and natural waters. Nanomaterials 9, 1–15. https://doi.org/10.3390/nano9030472.

Lead, J.R., Batley, G.E., Alvarez, P.J.J., Croteau, M.N., Handy, R.D., McLaughlin, M.J., Judy, J.D., Schirmer, K., 2018. Nanomaterials in the environment: Behavior, fate, bioavailability, and effects—an updated review. Environ. Toxicol. Chem. 37, 2029–2063. https://doi.org/10.1002/etc.4147.

Liu, Q., Lazouskaya, V., He, Q., Jin, Y., 2010. Effect of Particle Shape on Colloid Retention and Release in Saturated Porous Media. J. Environ. Qual. 39, 500–508. https://doi.org/10.2134/jeq2009.0100.

Liu, X., Wang, C., Wang, Zichen, Wu, Q., Wang, Zhi, 2015. Nanoporous carbon derived from a metal organic framework as a new kind of adsorbent for dispersive solid

phase extraction of benzoylurea insecticides. Microchim. Acta 182, 1903–1910. https://doi.org/10.1007/s00604-015-1530-8.
Lobel, B.T., Robertson, H., Webber, G.B., Ireland, P.M., Wanless, E.J., 2022. Impact of surface free energy on electrostatic extraction of particles from a bed. J. Colloid Interface Sci. 611, 617–628.
Lu, P.J., Fang, S.W., Cheng, W.L., Huang, S.C., Huang, M.C., Cheng, H.F., 2018. Characterization of titanium dioxide and zinc oxide nanoparticles in sunscreen powder by comparing different measurement methods. J. Food Drug Anal. 26, 1192–1200. https://doi.org/10.1016/j.jfda.2018.01.010.
Ma, H., Bolster, C., Johnson, W.P., Li, K., Pazmino, E., Camacho, K.M., Anselmo, A.C., Mitragotri, S., 2020. Coupled influences of particle shape, surface property and flow hydrodynamics on rod-shaped colloid transport in porous media. J. Colloid Interface Sci. 577, 471–480. https://doi.org/10.1016/j.jcis.2020.05.022.
Ma, X., Wigington, B., Bouchard, D., 2010. Fullerene C60: surface energy and interfacial interactions in aqueous systems. Langmuir 26 (14), 11886–11893.
Mitchelmore, C.L., He, K., Gonsior, M., Hain, E., Heyes, A., Clark, C., Younger, R., Schmitt-Kopplin, P., Feerick, A., Conway, A., Blaney, L., 2019. Occurrence and distribution of UV-filters and other anthropogenic contaminants in coastal surface water, sediment, and coral tissue from Hawaii. Sci. Total Environ. 670, 398–410. https://doi.org/10.1016/j.scitotenv.2019.03.034.
Mohammed, Y.H., Holmes, A., Haridass, I.N., Sanchez, W.Y., Studier, H., Grice, J.E., Benson, H.A.E., Roberts, M.S., 2019. Support for the safe use of zinc oxide nanoparticle sunscreens: lack of skin penetration or cellular toxicity after repeated application in volunteers. J. Invest. Dermatol. 139, 308–315. https://doi.org/10.1016/j.jid.2018.08.024.
NHMRC, NRMMC, 2011. Australian Drinking Water Guidelines Paper 6 National Water Quality Management Strategy. National Health and Medical Research Council, National Resource Management Ministerial Council, Commonwealth of Australia, Canberra.
Osmond, M.J., McCall, M.J., 2010. Zinc oxide nanoparticles in modern sunscreens: An analysis of potential exposure and hazard. Nanotoxicology 4, 15–41. https://doi.org/10.3109/17435390903502028.
Peng, X., Palma, S., Fisher, N.S., Wong, S.S., 2011. Effect of morphology of ZnO nanostructures on their toxicity to marine algae. Aquat. Toxicol. 102, 186–196. https://doi.org/10.1016/j.aquatox.2011.01.014.
Petosa, A.R., Jaisi, D.P., Quevedo, I.R., Elimelech, M., Tufenkji, N., 2010. Aggregation and deposition of engineered nanomaterials in aquatic environments: role of physicochemical interactions. Environ. Sci. Technol. 44, 6532–6549. https://doi.org/10.1021/es100598h.
Rajput, V.D., Minkina, T.M., Behal, A., Sushkova, S.N., Mandzhieva, S., Singh, R., Gorovtsov, A., Tsitsuashvili, V.S., Purvis, W.O., Ghazaryan, K.A., Movsesyan, H.S., 2018. Effects of zinc-oxide nanoparticles on soil, plants, animals and soil organisms: a review. Environ. Nanotechnol. Monit. Manag. 9, 76–84. https://doi.org/10.1016/j.enmm.2017.12.006.
Ramos, S., Homem, V., Alves, A., Santos, L., 2016. A review of organic UV-filters in wastewater treatment plants. Environ. Int. 86, 24–44. https://doi.org/10.1016/j.envint.2015.10.004.
Reyes-Herrera, J., Acosta-Slane, D., Castillo-Michel, H., Del Real, A.E.P., Vogel-Mikus, K., Benetti, F., Roman, M., Villanova, J., Valles-Aragón, M.C., 2022. Detection and characterization of TiO2 Nanomaterials in sludge from wastewater treatment plants of Chihuahua State, Mexico. Nanomaterials 12. https://doi.org/10.3390/nano12050744.
Rouquerol, F., Ruoquerol, J., Sing, K., 1999. Chapter1: Introduction. Adsorpt. by Powders Porous Solids. Academic Press, London, pp. 1–26.
Selck, H., Handy, R.D., Fernandes, T.F., Klaine, S.J., Petersen, E.J., 2016. Nanomaterials in the aquatic environment: A European Union-United States perspective on the status of ecotoxicity testing, research priorities, and challenges ahead. Environ. Toxicol. Chem. 35, 1055–1067. https://doi.org/10.1002/etc.3385.
Smijs, T.G., Pavel, S., 2011. Titanium dioxide and zinc oxide nanoparticles in sunscreens: Focus on their safety and effectiveness. Nanotechnol. Sci. Appl. 4, 95–112. https://doi.org/10.2147/nsa.s19419.
Stuart, B.H., Hunt, B.H., 2004. Infrared spectroscopy: Fundamentals and applications. Infrared Spectroscopy: Fundamentals and Applications. John Wiley & Sons Ltd, pp. 1–224. https://doi.org/10.1002/0470011149.
Tan, M., Qiu, G., Ting, Y.P., 2015. Effects of ZnO nanoparticles on wastewater treatment and their removal behavior in a membrane bioreactor. Bioresour. Technol. 185, 125–133. https://doi.org/10.1016/j.biortech.2015.02.094.
Tufenkji, N., Elimelech, M., 2004. Deviation from the classical colloid filtration theory in the presence of repulsive DLVO interactions. Langmuir 20, 10818–10828. https://doi.org/10.1021/la0486638.
Wang, D., Chen, Y., 2016. Critical review of the influences of nanoparticles on biological wastewater treatment and sludge digestion. Crit. Rev. Biotechnol. 36, 816–828. https://doi.org/10.3109/07388551.2015.1049509.
Yang, X., Wang, Q., Qu, X., Jiang, W., 2017. Bound and unbound humic acids perform different roles in the aggregation and deposition of multi-walled carbon nanotubes. Sci. Total Environ. 586, 738–745. https://doi.org/10.1016/j.scitotenv.2017.02.050.
Yotsumoto, H., Yoon, R.H., 1993. Application of extended DLVO theory. II. Stability of silica suspensions. J. Colloid Interface Sci. https://doi.org/10.1006/jcis.1993.1206.
Yung, M.M.N., Mouneyrac, C., Leung, K.Y.M., 2014. Ecotoxicity of zinc oxide nanoparticles in the marine environment. Encycl. Nanotechnol. 1–17. https://doi.org/10.1007/978-94-007-6178-0.
Zak, A.K., Razali, R., Majid, W.H.A., Darroudi, M., 2011. Synthesis and characterization of a narrow size distribution of zinc oxide nanoparticles. Int. J. Nanomedicine 6, 1399–1403. https://doi.org/10.2147/ijn.s19693.
Zhang, Y., Chen, Y., Westerhoff, P., Crittenden, J., 2009. Impact of natural organic matter and divalent cations on the stability of aqueous nanoparticles. Water Res. 43, 4249–4257. https://doi.org/10.1016/j.watres.2009.06.005.
Zheng, X., Yang, L., Shen, Q., Zhou, C., 2019. Evaluation of zinc oxide nanoparticles-induced effects on nitrogen and phosphorus removal from real and synthetic municipal wastewater. Ind. Eng. Chem. Res. 58, 7929–7936. https://doi.org/10.1021/acs.iecr.9b00641.
Zhou, Y., Fang, X., Gong, Y., Xiao, A., Xie, Y., Liu, L., Cao, Y., 2017. The interactions between zno nanoparticles (NPs) and α-linolenic acid (LNA) complexed to BSA did not influence the toxicity of ZnO NPs on HepG2 cells. Nanomaterials 7, 1–15. https://doi.org/10.3390/nano7040091.